



Push the Boundary of SAM: A Pseudo-label Correction Framework for Medical Segmentation

Ziyi Huang^{a,1}, Hongshan Liu^{b,c,1}, Haofeng Zhang^d, Xueshen Li^{b,c}, Haozhe Liu^{b,c}, Fuyong Xing^e, Andrew F. Laine^f, Elsa D. Angelini^{f,g,h}, Christine P. Hendon^{a,*}, Yu Gan^{b,c,*}

^aDepartment of Electrical Engineering, Columbia University, New York, NY 10027 USA

^bDepartment of Biomedical Engineering, Stevens Institute of Technology, Hoboken, NJ 07030 USA

^cCenter for Health Innovation, Stevens Institute of Technology, Hoboken, NJ 07030 USA

^dDepartment of Industrial Engineering and Operations Research, Columbia University, New York, NY 10027 USA

^eDepartment of Biostatistics and Informatics, Colorado School of Public Health, University of Colorado Anschutz Medical Campus, Aurora CO 80045, USA

^fDepartment of Biomedical Engineering, Columbia University, New York, NY 10027 USA

^gNIHR Imperial Biomedical Research Centre and ITMAT Data Science Group, Imperial College London, SW7 2BX London, U.K.

^hTelecom Paris, LTCI, Institut Polytechnique de Paris, 91120 Palaiseau, France

ARTICLE INFO

Article history:

Received 20 Dec 2023

Received in final form XXX

Accepted YYY

Available online ZZZ

Communicated by AAA

2000 MSC: 41A05, 41A10, 65D05, 65D17

Keywords: Segment Anything Model, Deep Learning, Image Analysis, Uncertainty, Weakly Supervised Learning

ABSTRACT

Segment anything model (SAM) has emerged as the leading approach for zero-shot learning in segmentation tasks, offering the advantage of avoiding pixel-wise annotations. It is particularly appealing in medical image segmentation, where the annotation process is laborious and expertise-demanding. However, the direct application of SAM often yields inferior results compared to conventional fully supervised segmentation networks. An alternative approach is to use SAM as the initial stage to generate pseudo labels for further network training. However, the performance is limited by the quality of pseudo labels. In this paper, we propose a novel label correction framework to push the boundary of SAM-based segmentation. Our model utilizes a label quality evaluation module to distinguish between noisy labels and clean labels. This enables the correction of the noisy labels using an uncertainty-based self-correction module, thereby enriching the clean training set. Finally, we retrain the segmentation network with updated labels to optimize its weights for future predictions. One key advantage of our model is its ability to train deep networks using SAM-generated pseudo labels without relying on a set of expert-level annotations while attaining good segmentation performance. We demonstrate the effectiveness of our proposed model on three public datasets, indicating its ability to improve segmentation accuracy and outperform baseline methods in label correction.

© 2023 Elsevier B. V. All rights reserved.

The code is available at <https://github.com/YGanLab/Pseudo-label-Correction-Framework>

*Corresponding author: cpf2115@columbia.edu, Department of Electrical Engineering, Columbia University, New York, NY 10027 USA (C.P. Hendon). ygan5@stevens.edu, Department of Biomedical Engineering, Stevens Institute of Technology, Hoboken, NJ 07030 USA (Y. Gan).

¹Equally contributed first authors

1. Introduction

The recent success of the segment anything model (SAM) (Kirillov et al., 2023) in the field of image segmentation sparks numerous discussions in computer vision (Zhang et al., 2023a; Wang et al., 2023; Mo and Tian, 2023; Ji et al., 2023a). Segment anything model, with a zero-shot setting, was trained on diverse data, including over a billion masks. One of its signifi-

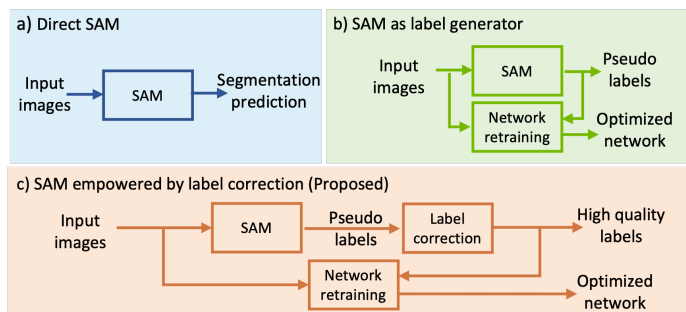


Fig. 1: A high-level comparison between existing SAM-based methods (a, b) and our proposed method (c).

cant advantages lies in its ability to segment without pixel-wise manual annotation, which is particularly appealing in medical image segmentation, considering the laborious and expertise-demanding nature of annotation.

However, directly deploying SAM on medical segmentation tasks, the methods shown in Fig. 1(a), has shown generally lower performance in comparison with state-of-the-art segmentation models like U-Net (Shi et al., 2023; Cheng et al., 2023; Deng et al., 2023; He et al., 2023a; Roy et al., 2023), despite its superior performance on natural images. Medical image segmentation presents unique challenges due to factors such as comparatively low signal-to-noise ratio, blurry boundaries, and salient features, making it a more intricate task compared to segmentation in natural image data. Consequently, pushing the limits of SAM in medical segmentation remains a particularly challenging endeavor.

In most of the medical datasets, there exists a significant performance gap between SAM segmentation and fully-supervised segmentation prediction. To bridge this gap, a new trend has emerged, wherein SAM is leveraged as a pseudo label generator for fully-supervised segmentation models (Zhang et al., 2023b; Sun et al., 2023; Hu and Li, 2023; Li et al., 2023) or network finetuning (Cui et al., 2023), as shown in Fig. 1(b). These approaches involve passing the data through a conventional segmentation network to hold on to the zero-shot nature of SAM, thus eliminating the need for pixel-wise annotations. Although the combination of SAM and fully supervised segmentation exhibits great promise, the performance is constrained by the quality of pseudo-labels generated by SAM, as the imperfect low-quality pseudo-labels can negatively impact the performance of the subsequent segmentation model, leading to lower segmentation performance.

To address the above issues, we propose a label correction framework to push the boundary of SAM-based segmentation as shown in Fig. 1(c). Inspired by the principle of self-supervised learning technique, our proposed framework can effectively correct pseudo-labels generated from SAM, improving the subsequent segmentation network to be resilient to imperfect annotation during the supervised training process and thus holding promise to improve their performance. A comparison between our proposed method and the existing SAM-based methods is shown in Fig. 1.

Within the domain of self-supervised learning against label noise (also called robust learning), existing advances mainly focused on image-level classification (Goldberger and Ben-Reuven, 2017; Hendrycks et al., 2018; Patrini et al., 2017; Jindal et al., 2016; Sukhbaatar et al., 2015; Wang et al., 2020b; Quan et al., 2020; Zhang et al., 2020b), which cannot be easily extended to segmentation tasks with pixel-wise predictions. On the pixel level, Wang et al. (Wang et al., 2020a) assigned small weights on noisy pixels based on training an additional meta mask network. Zhang et al. (Zhang et al., 2020a) applied a confident learning technique to characterize label noises from the training data to generate pixel-level noise identification maps. Zhu et al. (Zhu et al., 2019) proposed a framework to examine the label quality and assign different weights to the noisy labels at the image level. The work (Mirikharaji et al., 2019) considered the spatial variations in the quality of pixel-level annotations to learn spatially adaptive weight maps and adjusted the contribution of each pixel in the optimization of deep networks. Our previous work (Huang et al., 2021) generalized the structure of co-teaching (Han et al., 2018) into segmentation tasks by training two segmentation networks simultaneously to pick clean image samples for each one. However, a noteworthy limitation of those methods is that they rely on a subset of expensive expert-level clean labels during training. In practice, this is not feasible when working with SAM-generated pseudo-labels, as no expert-level supervision is involved in the process.

In this paper, we propose a novel label correction framework for SAM-generated pseudo-label improvement. The framework consists of the following three modules: label quality evaluation and reweighting module, self-correction module, and retraining module. In the first module, we design a multi-level reweighting strategy to automatically justify the label quality at the image level, thus eliminating the need for predefined clean image-level labels in a separate set. Benefiting from it, our proposed approach does not require any subset of human-annotated clean labels or predefined high-fidelity labels. After getting the confidence prediction from the label quality evaluation module, the self-correction module automatically corrects the noisy labels, enriching the high-quality pseudo labels for further training. Finally, we design a retraining module so that the network can benefit from the whole training set.

To the best of our knowledge, we propose the first label correction framework for SAM segmentation. Specifically, our main contributions include:

- (1) We propose a pseudo-label correction framework to push the boundary of SAM-based segmentation for medical images. The whole framework largely increases the performance of the SAM-based segmentation framework while holding the nature of zero-shot, i.e., no pixel-wised human-made annotation involved in training.
- (2) We develop a multi-level reweighting strategy for robust training against low-quality labels without any assumptions required for human-annotated clean or predefined high-fidelity labels, which is a particular fit for SAM-generated pseudo labels.
- (3) We experimentally demonstrate that our model significantly outperforms the existing SAM-based methods in three public datasets, boosting the performance of zero-shot learning

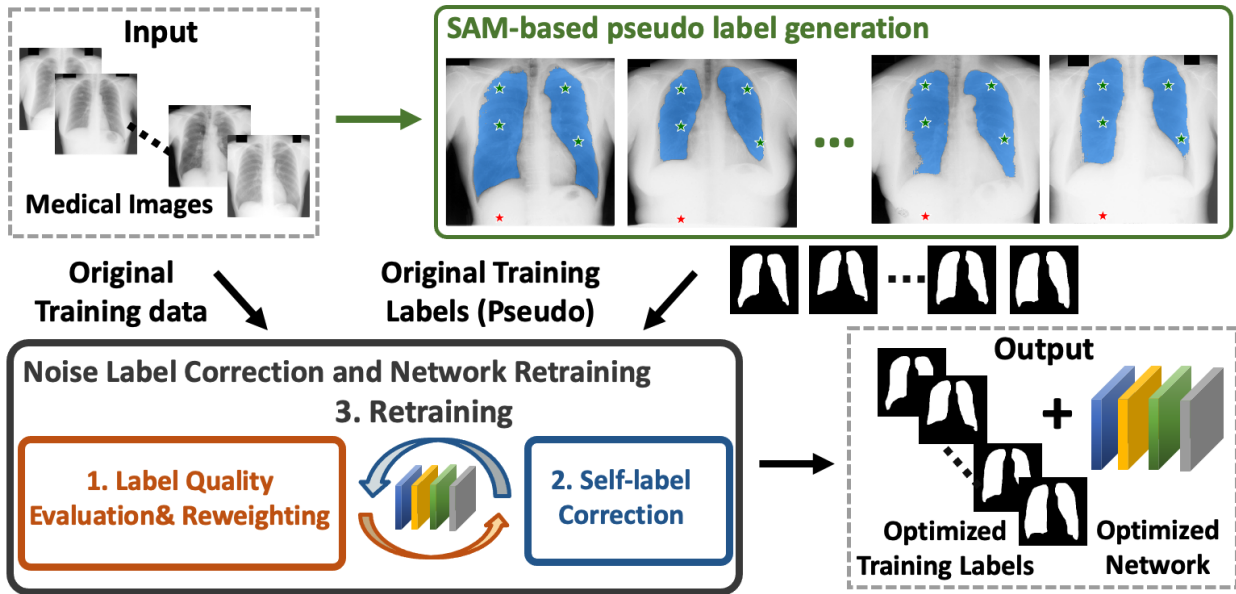


Fig. 2: Overview of proposed model. Given input medical images, our framework generates pseudo labels using SAM. The quality of pseudo labels is optimized for supervised learning. In SAM-based pseudo label generation, the green stars and red stars indicate positive and negative point prompts.

towards fully supervised learning.

2. Related work

2.1. Segment Anything Model in Medical Segmentation

Due to the difference between natural data and medical data, the ability of SAM to segment medical images that demand professional knowledge is limited. Directly applying SAM to real-world medical scenarios generates unsatisfying results compared to state-of-the-art segmentation performance (He et al., 2023a; Roy et al., 2023; Ji et al., 2023b; Zhang and Jiao, 2023; Chen et al., 2023; Zhang et al., 2023b; Cheng et al., 2023; Deng et al., 2023). Leveraging this foundational model to facilitate medical image segmentation still holds great promise. The masks generated by SAM can effectively provide coarse labels, serving as invaluable annotation tools for developing a precise and effective medical image segmentation model (Zhang et al., 2023b; Hu and Li, 2023; Li et al., 2023). However, the performance of the segmentation is not ideal or close to fully-supervised learning.

2.2. Label Correction in Segmentation

Zhu et al. (Zhu et al., 2020) proposed an organ segmentation model that used atlases to estimate the label deformation and used a fully convolution network to learn the relationship between image patches and measure the confidence of each patch and correct wrong labels. A pseudo-label correction framework that corrects the label at pixel-level and image-level was employed by Wu et al. (Wu et al., 2022), and this framework can correct the falsely predicted pixel labels and missed predicted pixel labels by a two-branch architecture, so as to improve the recall and precision. Yi et al. (Yi et al., 2021) addressed pixel-level noisy label segmentation problem by graph-based label

noise detection and correction framework, where the spatial adjacency and semantic similarity constraints are used to construct superpixel-based graph of the image and the clean labels are propagated to the noisy labels using a graph attention network. Ibrahim et al. (Ibrahim et al., 2020) used the ancillary model and primary model with weak annotation and strong annotation, and fused the features from two models by self-correcting module. A similar idea of early learning and label correction was further explored by Feng et al. (Feng et al., 2023), where a unified inflection hyperparameter was used to decide the label updating timing along with the training of an exponential moving average model. However, those methods are not optimized for medical image analysis.

2.3. Self-supervised Learning in Medical Image Segmentation

Supervised segmentation deep learning poses the need for labeled training data, which is costly in the medical image segmentation field, as domain expertise and large data scales are highly preferred. Self-supervised learning can accommodate this issue by training on unlabeled data. Kalapos et al. (Kalapos and Gyires-Tóth, 2023) investigated the transfer learning capability of self-supervised pretraining approaches for the downstream medical image segmentation tasks. Ouyang et al. (Ouyang et al., 2022) proposed a superpixel-based self-learning strategy and an adaptive local prototype pooling network that performed well in the few-shot medical image segmentation. Recently, Liu et al. (Liu et al., 2022) exploited the early learning behavior of semantic segmentation under noisy pixel-level labels and proposed a label correction strategy that is adaptive to early learning to improve the segmentation performance.

3. Methodology

Our goal is to automatically correct imperfect pseudo labels generated from SAM in training a segmentation network. As illustrated in Fig. 2, pseudo labels are generated using SAM. Then, our proposed method contains three modules to detect and correct low-quality labels for network training: (1) label quality evaluation and reweighting, (2) self-correction, and (3) retraining. Step (1) trains an initial segmentation network by weighing an subset of high-quality pixel and labels. Step (2) enriches the size of reliable dataset by correcting low-quality pixel to high-quality, namely label correction. Step (3) retrains the segmentation network by the improved dataset with updated labels.

3.1. Segment Anything Model in Label Generation

We choose to utilize the existing SAM model (Kirillov *et al.*, 2023) to generate pseudo labels for the training of a supervised segmentation network. The SAM model comprises three main components. Firstly, for the image encoder, Vision Transformer (Dosovitskiy *et al.*, 2020) pretrained with mean absolute error (MAE) is used to process the input image. Secondly, a prompt encoder is employed to process sparse and dense prompts. The stars, as shown in Fig. 2, are represented by positional encodings, and the masks are embedded by convolutions. Lastly, the mask decoder consists of a modified transformer decoder block and a dynamic prediction head.

To facilitate effective relation exploration between prompts and prompt-image, SAM employs prompt self-attention and prompt-image two-way cross-attention mechanisms, which subsequently update the embeddings. The output token is then mapped to the dynamic linear classifier by maximum a posterior (MAP) estimation after two decoder blocks, resulting in the output of the mask foreground probability. Consequently, a pseudo label is generated considering the tissue region in medical images.

3.2. Label Quality Evaluation and Reweighting Strategy

Definition of Noisy Labels. In medical segmentation, we term image with labels that have high fidelity with expensive and expert-level annotations (i.e., ground truth) as *clean image samples* and those pixels with labels that agree with expert-level annotation as *clean pixels*. Meanwhile, we term image samples that contain a subset of cheap unreliable annotations as *noisy image samples* and name those mis-labeled pixels (i.e., with labels different from ground truth) as *noisy pixels*. Note that in SAM-generated pseudo labels, there is no clean image label as SAM can not achieve a perfect segmentation performance with 100% accuracy (Cheng *et al.*, 2023; Deng *et al.*, 2023; He *et al.*, 2023a; Roy *et al.*, 2023). The number of noisy pixels within an image defines its “purity” at the image level.

In the following proposed framework, we establish a multi-level strategy to evaluate and reweight noisy labels simultaneously at image and pixel levels. Such strategy was designed to address noisy label caused by the nature of SAM image generation and consistent morphological similarities present across

medical images in segmentation tasks. In comparison with existing methods, we add image-level reweighting for two reasons. First, SAM generates pseudo labels on image-level basis. There are image frames that are generally underperformed in SAM-based label generation (example referred to Fig. 7(c)). These frames may lead to the presence of low-quality noisy labels surrounding individual clean pixels. The learning of local features and labels could mislead the network training. Secondly, in the context of medical segmentation tasks, there exists a morphological structural resemblance among various medical images. For instance, in lung X-ray images, both lung lobes are consistently positioned in the center. The noisy level at image level indicates how the network performs at similar segmentation regions at a macro-scale. Thus, it is important to have image level constraint on the cross image similarity in addition to pixel level-based reweighting.

Label Quality Evaluation. We evaluate the quality of training labels and detect low-quality label annotation using a segmentation neural network, as shown in Fig. 3. During the training phase, avoiding training on noisy pixels and noisy image samples can help to improve the robustness of the network against label corruption. Thus, in this module, we apply both image-level and pixel-level schemes for label quality evaluation to avoid performance degeneration. Considering that labels from clean pixels should be similar to the ground truth in terms of semantic structure, but noisy pixels do not, our module leverages cross entropy (CE) loss for noisy label detection and evaluation since it assesses the probabilistic similarity between the actual label and the predicted label. More specifically, pixels with large CE losses are likely to be noisy pixels, and image samples with large CE losses are likely to be low-quality. Therefore, we choose to detect and lower the weights of such pixels and images in the training procedure to help networks focus on learning from clean pixels and purer image samples. In particular, if we denote Ω as an image sample, the CE losses for an image sample Ω and a pixel x where $x \in \Omega$ are defined as follows, respectively:

$$L_{CE}(\Omega) = \sum_{x \in \Omega} L_{CE}(x) \quad (1)$$

$$L_{CE}(x) = - \sum_{l=1}^k g_l(x) \log(p_l(x)) \quad (2)$$

where k is the number of total classes, $p_l(x)$ provides the predicted probability of pixel x belonging to class l , and $g_l(x)$ is the one hot label for x .

Reweighting Strategy. Upon the detection of low-quality labels, we leverage a multi-level reweighting strategy to assign image samples and pixels with different weights. This multi-level reweighting strategy is designed to provide a multi-scale analysis on SAM-generated medical image masks. In particular, our reweighting strategy measures the pixel-level and image-level noises simultaneously. Along with the reweighting strategy, our total loss function is a combination of the pixel-wise weighted CE loss L_{CE} , the dice loss L_{Dice} , and the L_2 -regularization term on the parameters W of the network:

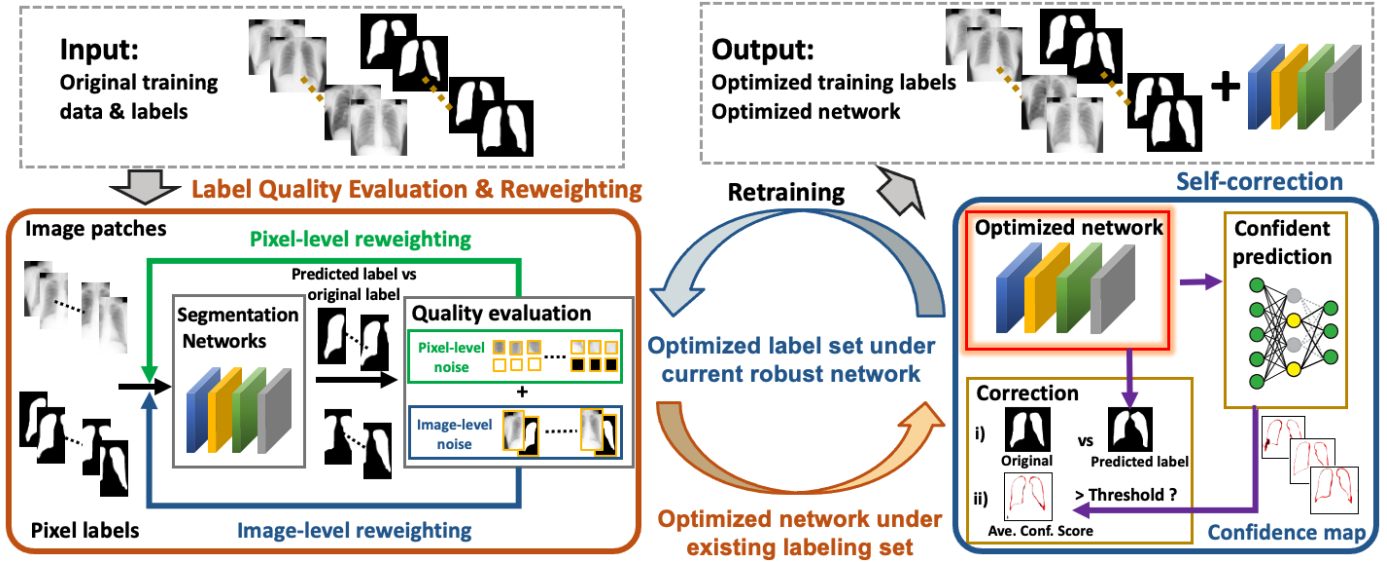


Fig. 3: The system flow of our proposed label correction model. Given training data and pseudo labels, our *label quality evaluation and reweighting* module adopts a multi-level reweighting strategy at both image-level and pixel level to robustly train the network against noisy labels. Based on the confidence prediction, the *self-correction* module corrects low-quality labels to enrich the clean set for further training. Benefiting from those two modules, a new network is retrained using the updated labels.

$$L_{total} = \sum_{\Omega} \lambda(\Omega) \left(\sum_{x \in \Omega} \alpha(x) L_{CE}(x) + L_{Dice}(\Omega) \right) + \|W\|_2^2, \quad (3)$$

$$L_{Dice}(\Omega) = 1 - \frac{1}{k} \sum_{l=1}^k \frac{2 \sum_{x \in \Omega} (p_l(x) g_l(x))}{\sum_{x \in \Omega} (p_l(x))^2 + \sum_{x \in \Omega} (g_l(x))^2}, \quad (4)$$

where $\alpha(x)$ is the pixel-wise weight assigned to the pixel x and $\lambda(\Omega)$ is the image-wise weight assigned to the image Ω . These weights are obtained from our novel multi-level reweighting strategy as described below.

Starting from the E_{start} -th epoch, we begin to assign pixel-wise weights $\alpha(x)$ and image-wise weights $\lambda(\Omega)$ on the training set to avoid overfitting to noisy labels. Intuitively, for an image sample that is severely low-quality with noisy pixels, the best way to avoid performance degeneration is to discard it. Thus, in the image-level reweighting scheme, we ignore the entire image sample Ω if it has a very large CE loss. The proportion of samples ignored in the training set is controlled by the forget rate, β . That is, in each mini-batch, we only select $1 - \beta$ percentage of samples with the smallest CE losses for network optimization.

For datasets containing a large number of noisy image samples, simply ignoring all of them will lead to severe overfitting, especially in biomedical applications. Thus, we further introduce a novel pixel-level reweighting scheme to assign different weights to each pixel. For a given noisy image sample Ω , pixels with large CE losses are more likely to be noisy pixels. Thus, we set $\alpha(x) = 0$ in Equation (3) if $L_{CE}(x) > q$, where q is the $1 - \gamma$ quantile of the set $\{L_{CE}(x) : x \in \Omega\}$, and $\alpha(x) = 1$ if $L_{CE}(x) \leq q$. The image-wise weight $\lambda(\Omega) = 1$ if the $L_{CE}(\Omega)$ ranks in the $1 - \beta$ smallest CE losses, otherwise $\lambda(\Omega) = 0$. Then, our network is optimized by the reweighted loss function, and on the next epoch, we recalculate the weights based

on the above strategy.

3.3. Self-Correction Module

Confidence Prediction. In the self-correction module, we selectively correct a subset of noisy labels based on confidence measurement in (Gal and Ghahramani, 2016). Inspired by (Hu et al., 2019; Sedai et al., 2018), we use the dropout-based Monte Carlo sampling approach to access the pixel-wise confidence information. In particular, we turn on dropout before each convolution layer and repeat Num stochastic forward passes of each training image through the network. In the j -th ($0 < j \leq Num$) forward pass, we compute the prediction vector $v^x = (v_1^x, v_2^x, \dots, v_{Num}^x)$ for each input pixel x . If the prediction of the x pixel coincides with the prediction of the x pixel using the network without dropout, then $v_j^x = 1$, otherwise $v_j^x = 0$. The confidence score CS^x is then defined as

$$CS^x = \frac{\sum_{j=1}^{Num} v_j^x}{Num} \quad (5)$$

Noticing that CS is based on element-wise computing on a pixel x , a confidence map can be formed for each training image, as shown in Fig. 3.

Self-Correction. The self-correction module aims to enrich the training dataset with more high-quality pseudo labels. A label in the training set is corrected only when the following two conditions are satisfied simultaneously: 1) there is a mismatch between the predicted and original label, and 2) the predicted label has a high confidence score. To avoid the case where pixels are mis-corrected, we rely upon the confidence score, CS^x , to justify whether we need to avoid the potential mis-correct of pixels. Only pixels that we confidently know the correct labels will be updated in the new training dataset. We expect the pixels with updated labels will be assigned a higher weight in future

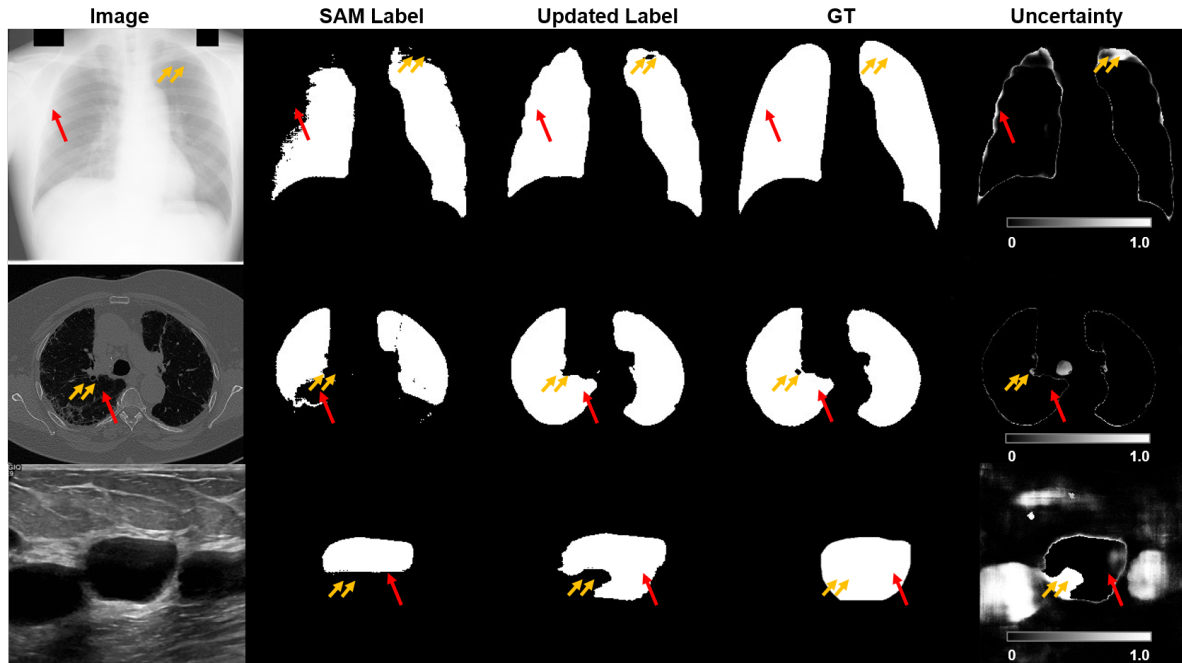


Fig. 4: Representative example of pseudo labels correction from both JSRT dataset (first row), lung CT dataset (second row), and BUSI dataset (third row). In each row, updated labels using our proposed method significantly convert noisy pixel labels to clean pixel labels. The red arrow highlights the corrected region. The yellow double arrows indicate a region with high uncertainty, leading to missed label updates.

reweighting and retraining, thus providing better guidance in supervised learning.

3.4. Retraining Module

After implementing label corrections, we re-input the updated training labels to a randomly initialized segmentation network and start a new training procedure. We will repeat the label quality evaluation and reweighting from the updated training dataset. A new parameter network, \hat{W} , will be output after the retraining. Similarly, this retraining procedure uses the loss function defined in Equation (3) by considering both image and pixel level. Then, this segmentation network, \hat{W} , will be used to make the final prediction for any testing data.

4. Experiments

4.1. Datasets

We conduct evaluations on three publicly available datasets: the X-ray dataset from the Japanese Society of Radiological Technology (JSRT) (Shiraishi et al., 2000), lung CT from the Open Source Imaging Consortium (OSIC) Kaggle dataset (Konya, 2020), and the Breast Ultrasound Images (BUSI) dataset (Al-Dhabyani et al., 2020).

The JSRT dataset consists of 247 grayscale chest radiographs. The ground-truth lung masks are obtained from the Serial Chest Radiographs (SCR) database (Van Ginneken et al., 2006). Each chest radiograph is a 2D image with a dimension of 1024×1024 pixels. Following the work in (He et al., 2019; Hwang and Park, 2017), our training set and testing sets are split by the ID number. Thus, our training set contains 124 samples

with odd numbers and the testing set contains 123 even numbered chest radiographs.

The lung CT dataset used in this work comprises 50 volumes of CT scans that primarily focus on the lung region. The ground truth is provided from the OSIC pulmonary fibrosis dataset (Li et al., 2022). Each CT scan is a 3D volume with a dimension of 768×768 pixels or 512×512 pixels in the axial plane, and the number of axial slices ranges from 17 to 408 among scans. In this work, each CT scan is treated as an independent sample. We validate the performance using a cross-validation setup by randomly splitting the whole dataset by volumes into two groups and rotating the training and testing between the two groups. Averaged results in cross-validation are reported.

The BUSI dataset (Walid Al-Dhabyani et al., 2020) includes 780 ultrasound images depicting normal, benign, and malignant cases, each with corresponding segmentation maps. The images are acquired from 600 female patients, with an average size of 500×500 pixels. For our study, we exclude images with landmarks and texts and utilize a subset of this dataset that consists of 647 benign and malignant images depicting cases of breast tumors. We randomly select 520 images for training and 127 images for testing.

4.2. Implementation Details.

In JSRT data, we resize all images from 1024×1024 pixels into 256×256 pixels and crop each image into small image patches with 256×128 pixels for data augmentation. In lung CT data, we resize the images from 768×768 or 512×512 into 256×256 pixels. Similarly, we crop each image into small image patches with 256×128 pixels. In BUSI dataset, we resize benign

and malignant images to 256×256 pixels. During the training, we used Adam optimizer (Kingma and Ba, 2014). The learning rate was initialized as 0.001 with the β_1 set as 0.9, and the β_2 set as 0.999. The learning rate was scheduled by a dynamic decay of the percentage of the rest epochs after 10 epochs. The β_1 was set as 0.1 after 10 epochs. In total, the networks were trained 300 epochs to ensure convergence. The quantile parameter was set as 0.05. We empirically set forget rate β as 20% for JSRT, 10% for lung CT data, and 10% for BUSI. We set the dropout number N as 100 for JSRT, 120 for lung CT data, and 100 for BUSI. The experiments were carried out in parallel on two RTX A6000 GPUs.

4.3. Label Correction Performance

We first evaluate the performance of label correction. In Fig. 4, we present three representative examples, from the JSRT dataset (first row), the lung CT dataset (second row), and BUSI dataset (third row) respectively, to show the label correction performance of our proposed model from the SAM-generated pseudo labels (denoted as SAM Label). Compared with the original pseudo labels, the corrected labels are more similar to the ground truth, showing a significant improvement in label quality. In addition, the boundaries get smoother, and the regions with missing pixels, where the red arrow points in each figure, are automatically corrected. In concordance with the results in (Kendall et al., 2015), the confidence maps (denoted as uncertainty) in Fig. 4 have higher uncertainty among the tissue boundaries, as shown in double arrows. It evidently shows that the confidence maps could accurately locate the hard pixels caused by the boundary ambiguity. Thus, our label correction module will not miscorrect those hard pixels which are difficult for the networks to make predictions.

Table 1 quantitatively compares the improvement of label quality. Against the ground truth, we compare the percentage of pixels that are clean in SAM-generated labels and updated labels. True positive (TP), false positive (FP), true negative (TN), and false negative (FN) are all calculated and compared. True positive rate is increased by 3.79% in JSRT, 4.55% in lung CT, and 3.54% in BUSI. This is considered a significant improvement because most of the updated labels occur at the boundary of the lung region, as shown in Fig 4. Moreover, we observe the decrease of FP and FN with TN increase as well. Our superior performance indicates that our model can push the limit of label quality, providing high-quality labels for the training of the segmentation network. It is worth mentioning that we observe a higher FP rate in the BUSI dataset compared to the JSRT and CT dataset, which is consistent with (Shen et al., 2021) where a high false positive rate for the BUSI dataset is reported due to a comparative low signal-to-noise ratio (SNR).

4.4. Comparative Studies on Segmentation Performance

We further evaluate the impact of label correction on prediction of segmentation task before and after retraining with updated labels. In particular, we compare the segmentation performance on the same testing dataset from the following methods: 1) Zero-shot segmentation directly from SAM (denoted as Direct SAM) (Kirillov et al., 2023); 2) Segmentation using SAM

Table 1: Label correction performance for SAM noise labels for JSRT, CT, and Ultrasound datasets.

		TP	FP	TN	FN
JSRT	SAM	81.58%	0.58%	99.42%	18.41%
	Updated label	85.37%	0.14%	99.86%	14.62%
	Difference	3.79% \uparrow	0.44% \downarrow	0.44% \uparrow	3.79% \downarrow
CT	SAM	88.57%	0.90%	99.10%	11.43%
	Updated label	93.12%	0.64%	99.36%	6.88%
	Difference	4.55% \uparrow	0.26% \downarrow	0.26% \uparrow	4.55% \downarrow
BUSI	SAM	61.43%	4.35%	95.64%	38.57%
	Updated label	64.97%	4.07%	95.92%	35.03%
	Difference	3.54% \uparrow	0.28% \downarrow	0.28% \uparrow	3.54% \downarrow

Enhanced Pseudo Labels (SEPL) (Chen et al., 2023); 3) Segmentation using adaptive early-learning correction (ADELE) (Liu et al., 2022); 4) Segmentation using pseudo labels without label correction (SAM-NLC) (Jiang and Yang, 2023); 5) Segmentation using pseudo label corrected from existing robust learning method, pixel-wise and image-level noise tolerant (SAM-PINT) (Shi and Wu, 2021); 6) Segmentation using our proposed multi-level label correction (SAM-MLC) method; 7) Segmentation using UNet (Ronneberger et al., 2015) with clean labels that are from expertise annotation (Seg-Noise Free). Except for SEPL (no training required) and SAM-NLC (adopt the implementation by (Jiang and Yang, 2023)), the rest of the segmentation methods are trained based on UNet (Ronneberger et al., 2015) structure to ensure a fair comparison. Among all methods, SAM-NLC represents the baseline of SAM-based zero-shot segmentation performance. Seg-Noise Free is the upper limit where all expertise labels are available, which is the ideal case but very challenging to obtain in medical image segmentation. We show representative images from the three datasets in Fig.5. We observe that the segmentation results obtained from directly using Direct SAM, SEPL, ADELE, and SAM-NLC are not satisfactory, as clusters of tissue boundary are misclassified as background when the boundary in the original image is blurry (red triangles). Moreover, the SEPL and ADELE tend to misclassify background regions into tissue regions (gold dash circle). Although the SAM-PINT could improve the performance slightly, it also has the issue of mistakenly classify background to foreground (gold dash circle). In contrast, our method (i.e., SAM-MLC) shows robustness in prediction results among the three datasets. The overall prediction performance is comparable with models trained from noise-free labels, and the segmentation results are consistent with the ground truth. Our method outperforms SAM-PINT because we consider multi-weight simultaneously, and we have a label correction module to enrich high-quality labels in the training dataset. We observe that the SEPL and ADELE demonstrate the worst performance for the BUSI dataset. We consider the SEPL and ADELE to rely on the quality of Direct SAM annotations. The SEPL and ADELE may produce a negative impact if the Direct SAM annotation has poor quality. In contrast, our method is capable of generating satisfactory results when the Direct SAM labels are less optimal.

A similar observation is found in Table. 2. We use both the Dice coefficient and accuracy to evaluate the segmentation performance. Overall, SAM-MLC brings the largest improve-

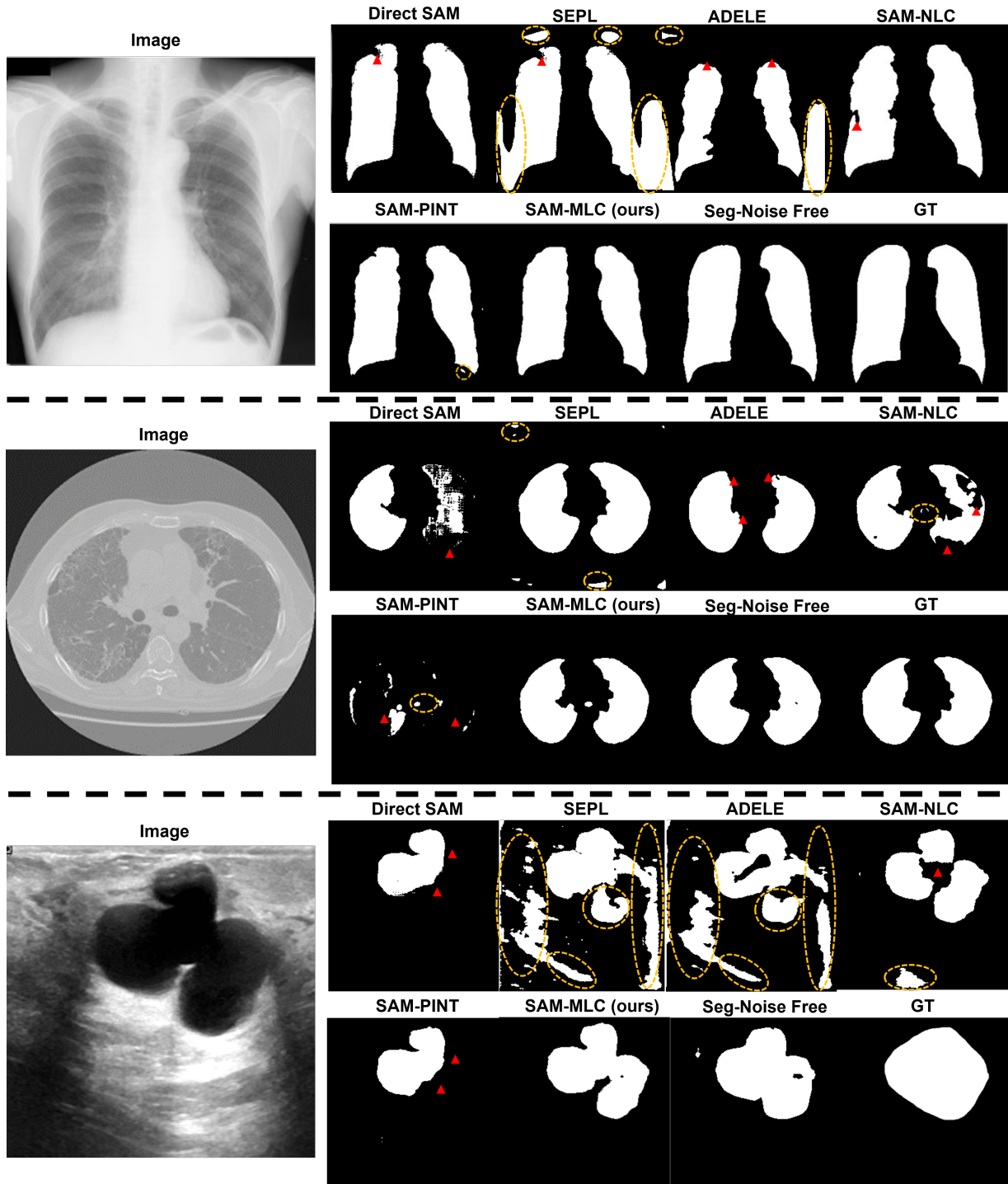


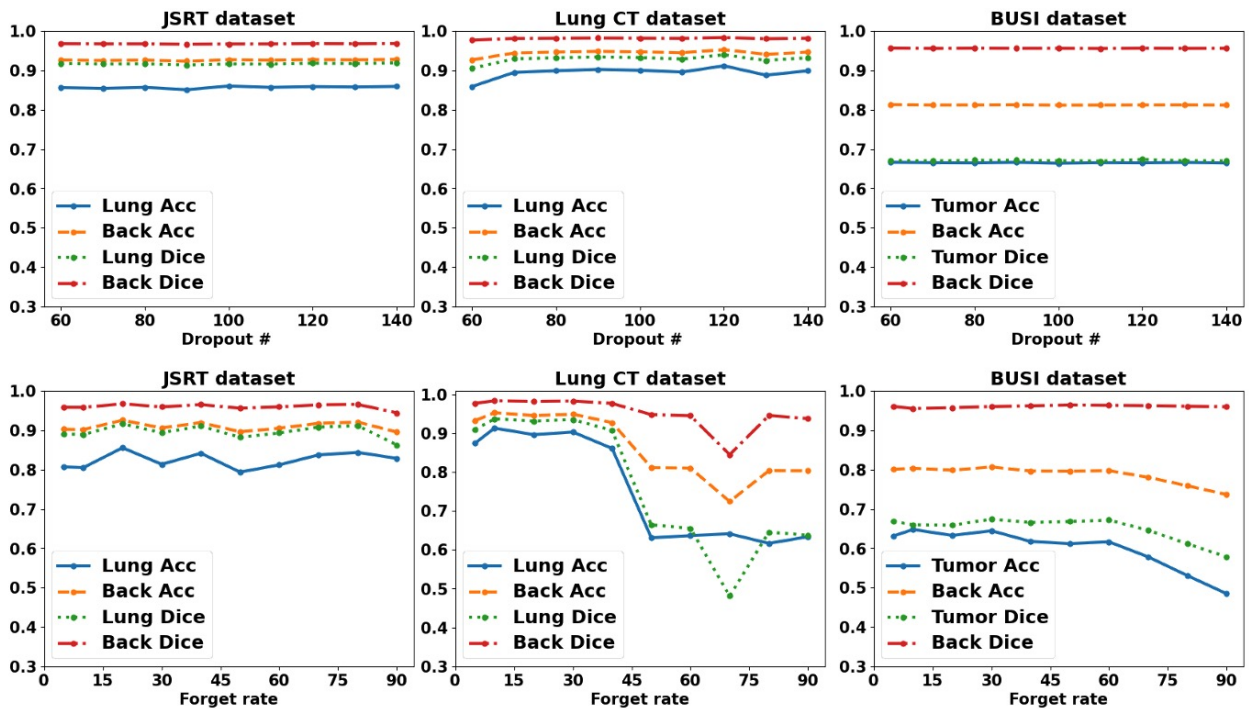
Fig. 5: Segmentation performance of the baseline methods and the proposed method from the JSRT dataset (first row), lung CT dataset (second row), and BUSI dataset (third row). With the multi-level label correction framework, our proposed method (SAM-MLC) outperforms the existing label correction method (SEPL, ADELE, and SAM-PINT) and achieves comparable segmentation performance to the fully supervised learning network from noise-free dataset (Seg-Noise Free). Red triangles indicate representative regions that are misclassified as background. Gold dash circles indicate representative regions that are misclassified as tissue regions.

ment from Direct SAM. In particular, in the CT dataset, the performance of SAM-MLC is only 2.79% (Acc for tissue) and 1.26% (Dice for tissue) lower than the ideal case when segmentation is trained from noise-free labels. Noticeably, the improvements in the X-ray (JSRT) dataset and ultrasound (BUSI)

are lower than the CT dataset. This is because the SNR is generally higher in CT (Computed Tomography) compared to conventional X-ray images and ultrasound images. Therefore, the boundary in X-ray and ultrasound images are blurrier than that in CT images, making it harder to correct pseudo-labels to ex-

Table 2: Evaluation metrics of different models on three dataset with noisy labels from SAM. Best results are in **bold**. The second best performance is underlined.

		JSRT		Lung CT		BUSI	
		Acc	Dice	Acc	Dice	Acc	Dice
Direct SAM (Kirillov et al., 2023)	Tissue	80.95%	88.50%	88.26%	91.44%	61.70%	64.78%
	Background	90.12%	95.53%	93.45%	97.58%	78.77%	95.17%
SEPL (Chen et al., 2023)	Tissue	63.49%	69.83%	85.79%	88.82%	62.78%	22.17%
	Background	81.58%	92.74%	92.49%	97.55%	69.89%	84.08%
ADELE (Liu et al., 2022)	Tissue	59.81%	64.33%	88.80%	90.04%	60.42%	24.44%
	Background	74.61%	86.32%	92.49%	96.65%	70.44%	86.25%
SAM-NLC (Jiang and Yang, 2023)	Tissue	78.71%	87.41%	87.30%	91.02%	46.87%	51.02%
	Background	89.18%	95.36%	93.19%	97.71%	72.95%	95.69%
SAM-PINT (Shi and Wu, 2021)	Tissue	81.68%	89.07%	88.01%	92.29%	48.12%	52.08%
	Background	90.62%	95.96%	93.61%	98.01%	72.95%	95.66%
SAM-MLC (ours)	Tissue	<u>85.51%</u>	<u>91.88%</u>	<u>92.70%</u>	<u>94.67%</u>	<u>66.04%</u>	<u>68.26%</u>
	Background	<u>92.65%</u>	<u>96.80%</u>	<u>95.98%</u>	<u>98.55%</u>	<u>81.42%</u>	<u>96.09%</u>
Seg-Noise Free (upper limit)	Tissue	97.96%	97.26%	95.49%	95.93%	76.24%	75.41%
	Background	98.61%	98.92%	97.28%	98.85%	87.25%	97.19%

Fig. 6: Effect of hyperparameter on the segmentation performance in JSRT dataset, lung CT dataset, and BUSI dataset. Forget rate β and dropout number N are evaluated. Lung Acc = Lung Accuracy; Back Acc = Background Accuracy; Tumor Acc = Tumor Accuracy; Lung Dic = Lung Dice Coefficient; Back Dice = Background Dice Coefficient.

performer level. Generally, the segmentation performances are the lower in the BUSI dataset (around 61% Dice score for Direct SAM prediction of tissue and around 77% Dice score for Seg-Noise Free prediction of tissue) than the performance in other two datasets. This is consistent with results presented in (He et al., 2023b). We believe that the under-performance of the BUSI dataset stems from two key factors: the lower SNR the ultrasound images and the inadequate quality of the ground truth data, where the annotator had challenges in accurately delineat-

ing boundaries of tumor region.

4.5. Effects of Hyperparameters

We also perform studies to evaluate the effects of two critical parameters, forget rate (β) and dropout number (N), on testing data, as shown in Fig. 6. Forget rate is a critical factor in reweighting module, determining the ratio of reliable samples used for reweighting. The dropout number is a critical factor in the self-correction module. We studied the performance with

Table 3: Evaluation metrics of our proposed model on the JSRT, CT, and BUSI dataset after removing (w/o) each module from our model under SAM noisy label.

		SAM-MLC (ours)		(1) w/o pixel weights		(2) w/o image weights		(3) w/o retraining	
		Acc	Dice	Acc	Dice	Acc	Dice	Acc	Dice
JSRT	Lung	85.51%	91.88%	81.42%	89.40%	82.51%	90.13%	83.69%	90.78%
	Background	92.65%	96.80%	90.64%	95.99%	91.17%	96.20%	91.76%	96.44%
CT	Lung	92.70%	94.67%	90.71%	93.37%	91.90%	94.39%	90.66%	93.78%
	Background	95.98%	98.55%	94.87%	98.23%	95.62%	98.47%	95.05%	98.35%
BUSI	Tumor	66.04%	68.26%	64.98%	66.86%	64.67%	67.09%	64.51%	67.46%
	Background	81.42%	96.09%	80.91%	96.05%	80.65%	95.92%	80.63%	95.97%

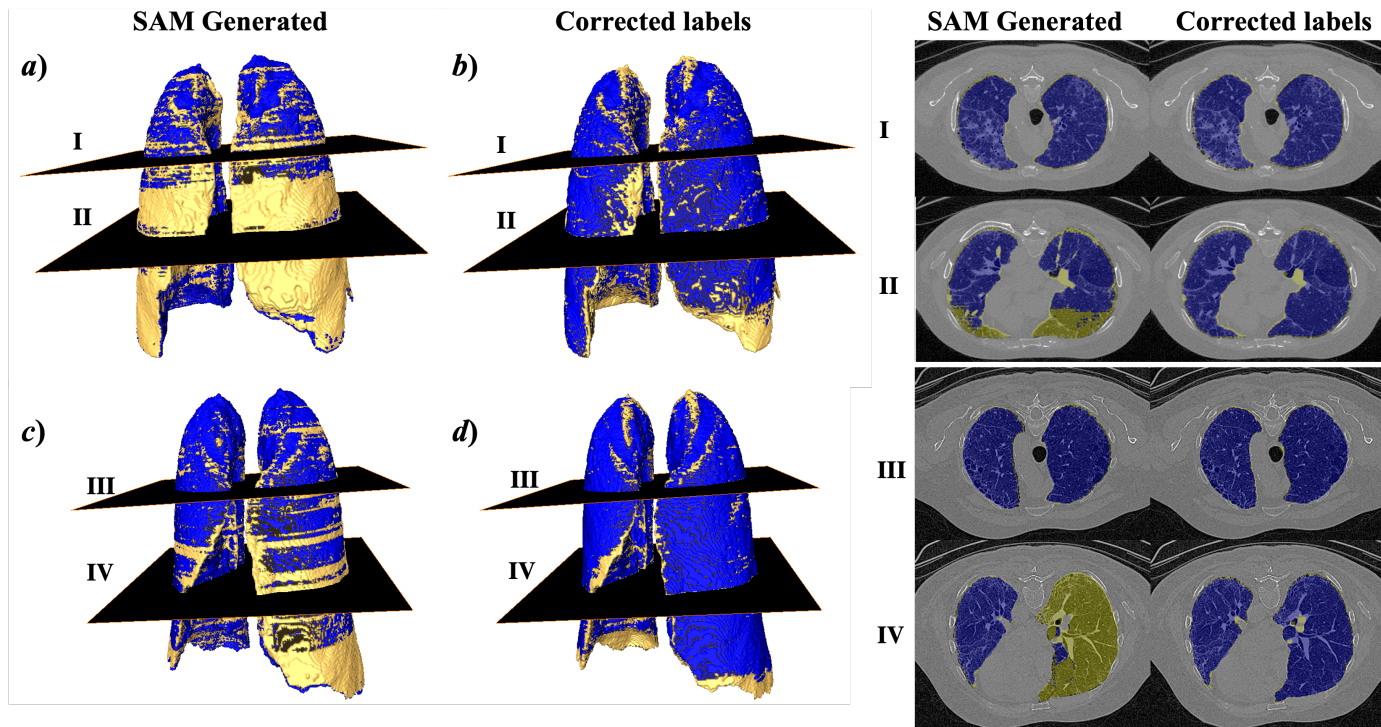


Fig. 7: Representative label correction performance in 3D. The SAM generated pseudo label is severely low quality in a) and corrected in b). The SAM generated pseudo label is mildly low quality in c) and corrected in d). Four cross-sectional 2D images from 3D visualization are shown in the right two panels. The labels are overlaid with original CT images. Yellow regions in both 3D and 2D visualization correspond to noisy pixels. Blue regions in both 3D and 2D visualization correspond to clean pixels.

forget rate from 5% to 90%, and with dropout number from 60 to 140 on three datasets. We found that for three datasets, the performances are stable with the forget rate in the range of 5% to 40% and with the dropout number in the range of 70 to 110, which demonstrates that the performance is robust against the selection of hyper-parameters among all dataset.

4.6. Ablation Study

To show the effectiveness of our proposed model, we further evaluate each module via ablation experiments on three datasets presenting the following four experiments, each removing a certain component of our model: (1) without the pixel-level reweighting strategy; (2) without the image-level reweighting strategy; (3) without the retraining module. The performance degenerates when any one of our modules is removed, showing the contribution of each module. Different from previous research, our reweighting strategy applies at both the image level and the pixel level. As shown in Table 3, particularly

in cases (1) and (2), this combined strategy can hugely improve the segmentation performance. The results from case (1) verify that our pixel-level reweighting strategy can effectively differentiate the mis-labeled pixels from the pixels with accurate annotations. The results from case (2) show that our network successfully avoids performance degeneration by ignoring severely corrupted samples via the image-level reweighting scheme. Moreover, in case (3), the accuracy drops significantly when the retraining module is removed. These results overall confirm the beneficial effect of the label correction module and the retraining module, indicating that the label correction module can effectively enrich the clean training set labels via updating noisy labels.

4.7. 3D Visualization

Figure 7 shows the 3D visualization of label correction from the CT dataset. We compare the distribution of noisy pixels (colored in yellow) and clean pixels (colored in blue) before and after label correction in 3D space. Cross-sectional image is

processed sequentially in 2D and then aligned in 3D. Figure 7 (a-b) shows a scenario where SAM generated labels are generally low quality around surface. From plane I, we observe that even the boundary region is noisy, the pixels in the inner region could be dominantly clean. Figure 7 (c-d) shows a scenario that is comparatively mild case of noise in 3D surface area. In plane IV, although the surface is not clustered with noisy image, the inner region (i.e., the right lobe) is severely noised. In such case, simply learning at pixel-level may learn incorrect boundary patterns. There is a need for learning at image-level such that labels that are severely corrupted can be minimally learned in training process. Overall, the pattern of consecutive corrupted frames highlights a multi-level reweight/learning strategy to consider label noise at image-level.

Four planes at the right two columns represent scenarios where noise pixels at mild (plane I and III), moderate (plane II), and severe (plane IV). In all scenarios, our label correction method successfully corrects a majority of noisy pixels and updates them to clean pixels. The corrected labels accurately delineate the morphological changes in the lung region tissues. The 3D segmentation visualization indicates great potential to evaluate the 3D morphology of lung regions and calculate metrics related to respiratory disease.

5. Discussion

In this study, we present a novel pseudo label correction framework to enhance the performance of SAM segmentation in medical images. This framework addresses the issue of low-quality pseudo labels in supervised learning and also takes advantage of zero-shot learning, in which no pixel-wised annotation is needed. Through multi-level reweighting and self-correction, we achieve significant improvements in segmentation performance compared to Direct SAM, effectively approaching the quality of fully supervised learning with expert-level annotations.

In the evaluation of label correction methods for medical segmentation, we specifically compare our framework with the SEPL (Chen et al., 2023), ADELE (Liu et al., 2022), and PINT (Shi and Wu, 2021). Unlike the SEPL and ADELE, our method updates the labels based on the calculation of label confidence during training. Our framework is different from PINT in three aspects. First, we handle low-weight pixels differently. Unlike PINT, which discards such pixels during training for robust learning, our approach corrects and updates these pixels with new labels. This augmentation of the training dataset with additional labels contributes to improved performance. Second, our framework includes an extra retraining module that refines the network through multiple runs with updated labels, in contrast to PINT's single network training. Third, while PINT employs a two-level sequential reweighting strategy, our approach conducts reweighting concurrently. PINT employs distinct phases of pixel-level and image-level noise-tolerant learning, whereas our method ensures computational efficiency and mitigates the accumulation of low-quality image-level errors between phases.

We did not compare it with other existing label correction methods such as (Zhu et al., 2019; Mirikharaji et al., 2019;

Han et al., 2018), including our previous work in (Huang et al., 2021). The reason is that those methods require a subset of images with predefined clean labels, which is not feasible to obtain with SAM-generated pseudo labels.

Noticeably, our enhanced performance incurs only minimal addition in computational cost. A single iteration of retraining is added, and there are no additional costs during online testing. This favorable characteristic makes our framework suitable for real-time diagnosis applications.

Furthermore, we demonstrate the generality and effectiveness of our framework on three medical datasets: an X-ray dataset, a lung CT dataset, and an ultrasound dataset. The results showcase the capability of our approach in correcting pseudo labels for lung structure as well as tumor tissue. In the future, we plan to validate our framework on more intricate tissue structures, such as airway structures and irregular cancer structures, further expanding its applicability and impact in medical image segmentation.

6. Conclusion

In this paper, we introduce a novel label correction learning framework designed to advance the boundaries of SAM-based medical segmentation. The proposed method jointly optimizes the network and the noisy training set. With special consideration on the pixel-wise and image-wise label quality, we apply a multi-level reweighting strategy for noise resistance and overfitting control. To improve the quality of labels, the self-correction module automatically corrects the noisy labels to enrich the clean pixels for further training.

Notably, the strength of our approach lies in its ability to enhance segmentation accuracy without relying on pixel-wise annotations. We validate the effectiveness of our label correction framework through comprehensive experiments on the JSRT X-ray dataset, lung CT dataset, and Ultrasound breast cancer dataset, demonstrating its capability to significantly improve segmentation results in medical image processing.

CRediT authorship contribution statement

ZH: Conceptualization, Methodology, Software, Validation, Formal analysis, Investigation, Data Curation, Visualization, Writing - Original Draft. **HS Liu:** Conceptualization, Methodology, Software, Validation, Formal analysis, Investigation, Data Curation, Visualization, Writing - Original Draft. **HZ:** Conceptualization, Methodology, Software. **XL:** Software, Validation, Formal analysis, Visualization, Investigation. **HZ Liu:** Software, Validation, Formal analysis, Visualization, Investigation, Data Curation. **FX:** Conceptualization, Methodology, Investigation, Writing - Review & Editing. **AFL:** Conceptualization, Methodology, Investigation, Writing - Review & Editing. **EDA:** Conceptualization, Methodology, Investigation, Writing - Review & Editing. **CPH:** Conceptualization, Formal analysis, Funding acquisition Investigation, Methodology, Project administration, Software, Supervision, Validation,

Visualization Writing – original draft, Writing – review & editing. **YG**: Conceptualization, Formal analysis, Funding acquisition Investigation, Methodology, Project administration, Software, Supervision, Validation, Visualization Writing – original draft, Writing – review & editing.

Declaration of competing interest

The authors declare that they have no conflict of interest.

Acknowledgments

Funding: This paper is supported in part by NIH-5R01HL14936 (CPH), Cheung-Kong Innovation Doctoral Fellowship (ZH), Stevens Provost Fellowship (HZ Liu), NSF-2222739(YG), NSF-2239810 (YG), New Jersey Health Foundation (YG), USDA/NIFA-2022-67021-36866 (YG).

References

- Al-Dhabyani, W., Gomaa, M., Khaled, H., Fahmy, A., 2020. Dataset of breast ultrasound images. *Data in brief* 28, 104863.
- Chen, T., Mai, Z., Li, R., Chao, W.L., 2023. Segment anything model (sam) enhanced pseudo labels for weakly supervised semantic segmentation. *ArXiv abs/2305.05803*. URL: <https://api.semanticscholar.org/CorpusID:258587943>.
- Cheng, D., Qin, Z., Jiang, Z., Zhang, S., Lao, Q., Li, K., 2023. SAM on medical images: A comprehensive study on three prompt modes. *arXiv preprint arXiv:2305.00035*.
- Cui, C., Deng, R., Liu, Q., Yao, T., Bao, S., Remedios, L.W., Tang, Y., Huo, Y., 2023. All-in-SAM: from weak annotation to pixel-wise nuclei segmentation with prompt-based finetuning. *arXiv preprint arXiv:2307.00290*.
- Deng, R., Cui, C., Liu, Q., Yao, T., Remedios, L.W., Bao, S., Landman, B.A., Wheless, L.E., Coburn, L.A., Wilson, K.T., et al., 2023. Segment anything model (SAM) for digital pathology: Assess zero-shot segmentation on whole slide imaging. *arXiv preprint arXiv:2304.04155*.
- Dosovitskiy, A., Beyer, L., Kolesnikov, A., Weissenborn, D., Zhai, X., Unterthiner, T., Dehghani, M., Minderer, M., Heigold, G., Gelly, S., et al., 2020. An image is worth 16x16 words: Transformers for image recognition at scale. *arXiv preprint arXiv:2010.11929*.
- Feng, J., Wang, X., Li, T., Ji, S., Liu, W., 2023. Weakly-supervised semantic segmentation via online pseudo-mask correcting. *Pattern Recognition Letters* 165, 33–38.
- Gal, Y., Ghahramani, Z., 2016. Dropout as a bayesian approximation: Representing model uncertainty in deep learning. in: *International Conference on Machine Learning*, pp. 1050–1059.
- Goldberger, J., Ben-Reuven, E., 2017. Training deep neural-networks using a noise adaptation layer. in: *ICLR*.
- Han, B., Yao, Q., Yu, X., Niu, G., Xu, M., Hu, W., Tsang, I., Sugiyama, M., 2018. Co-teaching: Robust training of deep neural networks with extremely noisy labels. in: *Advances in Neural Information Processing Systems*, pp. 8527–8537.
- He, S., Bao, R., Li, J., Grant, P.E., Ou, Y., 2023a. Accuracy of segment-anything model (SAM) in medical image segmentation tasks. *arXiv preprint arXiv:2304.09324*.
- He, S., Bao, R., Li, J., Stout, J.N., Bjørnerud, A., Grant, P.E., Ou, Y., 2023b. Computer-vision benchmark segment-anything model (sam) in medical images: Accuracy in 12 datasets. URL: <https://api.semanticscholar.org/CorpusID:258558130>.
- He, X., Yang, S., Li, G., Li, H., Chang, H., Yu, Y., 2019. Non-local context encoder: Robust biomedical image segmentation against adversarial attacks. in: *Proceedings of the AAAI Conference on Artificial Intelligence*, pp. 8417–8424.
- Hendrycks, D., Mazeika, M., Wilson, D., Gimpel, K., 2018. Using trusted data to train deep networks on labels corrupted by severe noise. in: *Bengio, S., Wallach, H., Larochelle, H., Grauman, K., Cesa-Bianchi, N., Garnett, R. (Eds.), Advances in Neural Information Processing Systems*, Curran Associates, Inc.
- Hu, C., Li, X., 2023. When SAM meets medical images: An investigation of segment anything model (SAM) on multi-phase liver tumor segmentation. *arXiv preprint arXiv:2304.08506*.
- Hu, S., Worrall, D., Knekt, S., Veeling, B., Huisman, H., Welling, M., 2019. Supervised uncertainty quantification for segmentation with multiple annotations. in: *International Conference on Medical Image Computing and Computer-Assisted Intervention*, Springer, pp. 137–145.
- Huang, Z., Zhang, H., Laine, A., Angelini, E., Hendon, C., Gan, Y., 2021. Co-seg: An image segmentation framework against label corruption. URL: <https://arxiv.org/pdf/2102.00523.pdf>, *arXiv:2102.00523*.
- Hwang, S., Park, S., 2017. Accurate lung segmentation via network-wise training of convolutional networks. in: *Deep Learning in Medical Image Analysis and Multimodal Learning for Clinical Decision Support*. Springer, pp. 92–99.
- Ibrahim, M.S., Vahdat, A., Ranjbar, M., Macready, W.G., 2020. Semi-supervised semantic image segmentation with self-correcting networks. in: *Proceedings of the IEEE/CVF conference on computer vision and pattern recognition*, pp. 12715–12725.
- Ji, G.P., Fan, D.P., Xu, P., Cheng, M.M., Zhou, B., Van Gool, L., 2023a. SAM struggles in concealed scenes—empirical study on “segment anything”. *arXiv preprint arXiv:2304.06022*.
- Ji, W., Li, J., Bi, Q., Li, W., Cheng, L., 2023b. Segment anything is not always perfect: An investigation of SAM on different real-world applications. *arXiv preprint arXiv:2304.05750*.
- Jiang, P.T., Yang, Y., 2023. Segment anything is a good pseudo-label generator for weakly supervised semantic segmentation. *arXiv preprint arXiv:2305.01275*.
- Jindal, I., Nokleby, M., Chen, X., 2016. Learning deep networks from noisy labels with dropout regularization. in: *2016 IEEE 16th International Conference on Data Mining (ICDM)*, IEEE, pp. 967–972.
- Kalapos, A., Gyires-Tóth, B., 2023. Self-supervised pretraining for 2D medical image segmentation. in: *Computer Vision—ECCV 2022 Workshops: Tel Aviv, Israel, October 23–27, 2022, Proceedings, Part VII*, Springer, pp. 472–484.
- Kendall, A., Badrinarayanan, V., Cipolla, R., 2015. Bayesian segnet: Model uncertainty in deep convolutional encoder-decoder architectures for scene understanding. *arXiv preprint arXiv:1511.02680*.
- Kingma, D.P., Ba, J., 2014. Adam: A method for stochastic optimization. *arXiv preprint arXiv:1412.6980*.
- Kirillov, A., Mintun, E., Ravi, N., Mao, H., Rolland, C., Gustafson, L., Xiao, T., Whitehead, S., Berg, A.C., Lo, W.Y., et al., 2023. Segment anything. *arXiv preprint arXiv:2304.02643*.
- Konya, 2020. Lung segmentation dataset. URL: <https://www.kaggle.com/sandorkonya/ct-lung-heart-trachea-segmentation>.
- Li, N., Xiong, L., Qiu, W., Pan, Y., Luo, Y., Zhang, Y., 2023. Segment anything model for semi-supervised medical image segmentation via selecting reliable pseudo-labels. Available at SSRN 4477443.
- Li, Z., Yang, L., Shu, L., Yu, Z., Huang, J., Li, J., Chen, L., Hu, S., Shu, T., Yu, G., et al., 2022. Research on CT lung segmentation method of preschool children based on traditional image processing and resnet. *Computational and Mathematical Methods in Medicine* 2022.
- Liu, S., Liu, K., Zhu, W., Shen, Y., Fernandez-Granda, C., 2022. Adaptive early-learning correction for segmentation from noisy annotations. in: *2022 IEEE/CVF Conference on Computer Vision and Pattern Recognition (CVPR)*, pp. 2596–2606.
- Mirikharaji, Z., Yan, Y., Hamarneh, G., 2019. Learning to segment skin lesions from noisy annotations. in: *Domain Adaptation and Representation Transfer and Medical Image Learning with Less Labels and Imperfect Data*. Springer, pp. 207–215.
- Mo, S., Tian, Y., 2023. Av-sam: Segment anything model meets audio-visual localization and segmentation. *arXiv preprint arXiv:2305.01836*.
- Ouyang, C., Biffi, C., Chen, C., Kart, T., Qiu, H., Rueckert, D., 2022. Self-supervised learning for few-shot medical image segmentation. *IEEE Transactions on Medical Imaging* 41, 1837–1848.
- Patrini, G., Rozza, A., Krishna Menon, A., Nock, R., Qu, L., 2017. Making deep neural networks robust to label noise: A loss correction approach. in: *Proceedings of the IEEE Conference on Computer Vision and Pattern Recognition*, pp. 1944–1952.
- Quan, L., Li, Y., Chen, X., Zhang, N., 2020. An effective data refinement approach for upper gastrointestinal anatomy recognition. in: *International Conference on Medical Image Computing and Computer-Assisted Intervention*, Springer, pp. 43–52.

- Ronneberger, O., Fischer, P., Brox, T., 2015. U-Net: Convolutional networks for biomedical image segmentation, in: International Conference on Medical image computing and computer-assisted intervention, Springer. pp. 234–241.
- Roy, S., Wald, T., Koehler, G., Rokuss, M.R., Disch, N., Holzschuh, J., Zimmerer, D., Maier-Hein, K.H., 2023. SAM.MD: Zero-shot medical image segmentation capabilities of the segment anything model. arXiv preprint arXiv:2304.05396 .
- Sedai, S., Antony, B., Mahapatra, D., Garnavi, R., 2018. Joint segmentation and uncertainty visualization of retinal layers in optical coherence tomography images using bayesian deep learning, in: Computational Pathology and Ophthalmic Medical Image Analysis. Springer. pp. 219–227.
- Shen, Y., Shamout, F.E., Oliver, J.R., Witowski, J., Kannan, K., Park, J., Wu, N., Huddleston, C., Wolfson, S., Millet, A., Ehrenpreis, R., Awal, D., Tyma, C., Samreen, N., Gao, Y., Chhor, C., Gandhi, S., Lee, C., Kumari-Subaiya, S., Leonard, C., Mohammed, R., Moczulski, C., Altabet, J., Babb, J., Lewin, A., Reig, B., Moy, L., Heacock, L., Geras, K.J., 2021. Artificial intelligence system reduces false-positive findings in the interpretation of breast ultrasound exams. *Nature Communications* 12, 5645. doi:10.1038/s41467-021-26023-2.
- Shi, J., Wu, J., 2021. Distilling effective supervision for robust medical image segmentation with noisy labels, in: Medical Image Computing and Computer Assisted Intervention–MICCAI 2021: 24th International Conference, Strasbourg, France, September 27–October 1, 2021, Proceedings, Part I 24, Springer. pp. 668–677.
- Shi, P., Qiu, J., Abaxi, S.M.D., Wei, H., Lo, F.P.W., Yuan, W., 2023. Generalist vision foundation models for medical imaging: A case study of segment anything model on zero-shot medical segmentation. *Diagnostics* 13, 1947.
- Shiraishi, J., Katsuragawa, S., Ikezoe, J., Matsumoto, T., Kobayashi, T., Komatsu, K.i., Matsui, M., Fujita, H., Kodera, Y., Doi, K., 2000. Development of a digital image database for chest radiographs with and without a lung nodule: receiver operating characteristic analysis of radiologists' detection of pulmonary nodules. *American Journal of Roentgenology* 174, 71–74.
- Sukhbaatar, S., Bruna, J., Paluri, M., Bourdev, L., Fergus, R., 2015. Training convolutional networks with noisy labels, in: 3rd International Conference on Learning Representations, ICLR 2015.
- Sun, W., Liu, Z., Zhang, Y., Zhong, Y., Barnes, N., 2023. An alternative to wsss? an empirical study of the segment anything model (sam) on weakly-supervised semantic segmentation problems. arXiv preprint arXiv:2305.01586 .
- Van Ginneken, B., Stegmann, M.B., Loog, M., 2006. Segmentation of anatomical structures in chest radiographs using supervised methods: a comparative study on a public database. *Medical Image Analysis* 10, 19–40.
- Walid Al-Dhabyani, Mohammed Gomaa, Hussien Khaled, Aly Fahmy, 2020. Dataset of breast ultrasound images. *Data in Brief* 28, 104863. URL: <https://www.sciencedirect.com/science/article/pii/S2352340919312181>, doi:10.1016/j.dib.2019.104863.
- Wang, D., Zhang, J., Du, B., Tao, D., Zhang, L., 2023. Scaling-up remote sensing segmentation dataset with segment anything model. arXiv preprint arXiv:2305.02034 .
- Wang, J., Zhou, S., Fang, C., Wang, L., Wang, J., 2020a. Meta corrupted pixels mining for medical image segmentation, in: International Conference on Medical Image Computing and Computer-Assisted Intervention, Springer. pp. 335–345.
- Wang, Z., Hu, G., Hu, Q., 2020b. Training noise-robust deep neural networks via meta-learning, in: Proceedings of the IEEE/CVF Conference on Computer Vision and Pattern Recognition, pp. 4524–4533.
- Wu, H., Wei, S., Tan, C., Zhao, Y., 2022. Pseudo-label correction from pixel to image, in: 2022 4th International Conference on Advances in Computer Technology, Information Science and Communications (CTISC), IEEE. pp. 1–5.
- Yi, R., Huang, Y., Guan, Q., Pu, M., Zhang, R., 2021. Learning from pixel-level label noise: A new perspective for semi-supervised semantic segmentation. *IEEE Transactions on Image Processing* 31, 623–635.
- Zhang, M., Gao, J., Lyu, Z., Zhao, W., Wang, Q., Ding, W., Wang, S., Li, Z., Cui, S., 2020a. Characterizing label errors: Confident learning for noisy-labeled image segmentation, in: International Conference on Medical Image Computing and Computer-Assisted Intervention, Springer. pp. 721–730.
- Zhang, R., Jiang, Z., Guo, Z., Yan, S., Pan, J., Dong, H., Gao, P., Li, H., 2023a. Personalize segment anything model with one shot. arXiv preprint arXiv:2305.03048 .
- Zhang, Y., Jiao, R., 2023. How segment anything model (SAM) boost medical image segmentation? arXiv preprint arXiv:2305.03678 .
- Zhang, Y., Zhou, T., Liang, P., Chen, D.Z., 2023b. Input augmentation with SAM: Boosting medical image segmentation with segmentation foundation model. arXiv preprint arXiv:2304.11332 .
- Zhang, Z., Zhang, H., Arik, S.O., Lee, H., Pfister, T., 2020b. Distilling effective supervision from severe label noise, in: Proceedings of the IEEE/CVF Conference on Computer Vision and Pattern Recognition, pp. 9294–9303.
- Zhu, H., Adeli, E., Shi, F., Shen, D., Initiative, A.D.N., 2020. FCN based label correction for multi-atlas guided organ segmentation. *Neuroinformatics* 18, 319–331.
- Zhu, H., Shi, J., Wu, J., 2019. Pick-and-learn: Automatic quality evaluation for noisy-labeled image segmentation, in: International Conference on Medical Image Computing and Computer-Assisted Intervention, Springer. pp. 576–584.